Gas Solubility in Hydrophobic Confinement

Alenka Luzar*,† and Dusan Bratko*,†,‡

Department of Chemistry, Virginia Commonwealth University, Richmond, Virginia 23284, and Department of Chemical Engineering, University of California, Berkeley, California 94720

Received: August 12, 2005; In Final Form: September 21, 2005

Measured forces between apolar surfaces in water have often been found to be sensitive to exposure to atmospheric gases despite low gas solubilities in bulk water. This raises questions as to how significant gas adsorption is in hydrophobic confinement, whether it is conducive to water depletion at such surfaces, and ultimately if it can facilitate the liquid-to-gas phase transition in the confinement. Open Ensemble molecular simulations have been used here to determine saturated concentrations of atmospheric gases in water-filled apolar confinements as a function of pore width at varied gas fugacities. For paraffin-like confinements of widths barely exceeding the mechanical instability threshold (spinodal) of the liquid-to-vapor transition of confined water (aqueous film thickness between three and four molecular diameters), mean gas concentrations in the pore were found to exceed the bulk values by a factor of ∼30 or ∼15 in cases of N_2 and CO_2, respectively. At ambient conditions, this does not result in visible changes in the water density profile next to the surfaces. Whereas the barrier to capillary evaporation has been found to decrease in the presence of dissolved gas (Leung, K.; Luzar, A.; and Bratko, D. *Phys. Rev. Lett.* **2003**, ***90***, 065502), gas concentrations much higher than those observed at normal atmospheric conditions would be needed to produce noticeable changes in the kinetics of capillary evaporation. In simulations, dissolved gas concentrations corresponding to fugacities above ∼40 bar for N_2, or ∼2 bar for CO_2, were required to trigger expulsion of water from a hydrocarbon slit as narrow as 1.4 nm. For nanosized pore widths corresponding to the mechanical instability threshold or above, no significant coupling between adsorption layers at opposing confinement walls was observed. This finding explains the approximately linear increase in gas solubility with inverse confinement width and the apparent validity of Henry's law in the pores over a broad fugacity range.

I. Introduction

Interfacial water pervades biological systems and plays a central role in geochemistry, environmental science, and numerous technologies. Because of its relation with the hydrophobic effect,[1] water in apolar confinements continues to represent a focus of intense experimental[2−4] and theoretical research.[5,6] There are significant qualitative differences between the hydrophobic solvation of smaller solutes and large hydrophobic particles.[7−14] For extended hydrophobic surfaces in water at ambient conditions (i.e., close to liquid−gas coexistence), the loss of hydrogen bonds,[15−18] the possibility that the liquid will recede from the surfaces (with a vapor layer separating the bulk phase from the surface), and the consequences of this phenomena (attractive depletion force[1]) have already attracted considerable attention.[11,19−26] The theory of Lum et al.[11] demonstrated that purely repulsive surfaces extending over 1 nm or more will nucleate a rather thick layer of depleted water density. Such an ideal and elegant statistical mechanical model[5] might have been a cause of some confusion in the recent experimental literature.[27] As pointed out by Stillinger,[7] a wide vapor film can develop when the external pressure is at or near the saturated vapor pressure. However, under common laboratory conditions, external pressure is atmospheric pressure, some 50 times the value of the saturated vapor pressure. The vaporlike layer in this case shrinks to *less* than a molecular diameter, as there are no forces preventing such a collapse. When the solute−solvent interactions are not just repulsive (hard-core)[7,11,28,29] but include attraction interactions, too,[30−36] the liquid will mostly adhere to the wall and only an insignificant depletion will be seen. The first direct measurement of dewetting of water next to a paraffin wall using X-ray reflectivity gave[37] an average deficit of about one molecule per 25−30 Å^2. A comparable (or weaker) water depletion follows from optical measurements on strongly hydrophobic silane-coated surfaces.[38] The proximity of another wall will, however, further destabilize the liquid phase and can give rise to capillary evaporation,[30,34,39−48] despite the fact that isolated weakly attractive walls do not display "drying" behavior. For typical hydrocarbon surfaces, the *vapor* phase is favored below separations of the order of 10^2 nm or more, although the liquid phase often persists at much smaller separations due to a significant kinetic barrier[34,39,41] to evaporation.

On the experimental side, our understanding of water-mediated surface interactions is largely based on surface-force measurements, either by the surface-force apparatus (SFA) or atomic force microscopy (AFM). Combining static *and dynamic* SFA and AFM techniques, it is possible to measure surface forces over the broad range of distances, from molecular scale to hundreds of nm.[1−4,49,50] Interpretations of hydrophobic forces rely on a variety of models for solute surfaces and intervening water, ranging from coarse-grained representations amenable to analytic approaches to molecular models used in simulations. Despite notable progress enabled through analysis and computer modeling, explaining certain features of interaction between

* E-mail: aluzar@vcu.edu (A.L) and dnb@berkeley.edu (D.B).
† Virginia Commonwealth University.
‡ University of California.

10.1021/jp054545x CCC: $30.25
Published on Web 11/08/2005

hydrophobic surfaces remains elusive.[51−54] Various mechanisms have been presumed to explain the long range of these forces, often significantly exceeding the range of molecular interactions within the aqueous phase. For globally neutral surfaces with regions of positive and negative charges, the observed long range has been suggested to be of electrostatic origin,[55] consistent with recent experimental studies.[4,56] In other contexts, it has been associated with the possibility of surface-induced liquid-to-vapor transitions (or local cavitation)[11,19−21,57−59] and with the effects of impurities, such as dissolved atmospheric gases.[54,60−73]

In most experiments and in nearly all situations of practical interest, water maintains equilibrium with the atmosphere and hence contains small amounts of dissolved gases, most notably N_2, O_2, and CO_2. The presence of gas can be felt in different ways: through nucleation of the supersaturated gas to nano- or microbubbles;[74−76] by enhanced depletion of water next to the surface;[73] as modulation of surface properties through adsorption;[66,77,78] or by facilitating water vapor nucleation[41] when the confined liquid is metastable[11,20,34,48,79] with respect to the gaseous phase. A number of experimental studies, including systematic surface force measurements, have revealed significant differences between the results obtained in the presence and absence of dissolved gases, with interaction typically being more attractive and longer ranged in water saturated by atmospheric gases.[60,63−65,72,73,80,81] Deaeration has invariably resulted in diminished long-range force.[72,80,81] To the extent that surface depletion of the solvent signifies increased attraction between surfaces,[22,23] recent neutron reflectivity measurement may suggest that a similar effect of dissolved gas persists at smaller surface separations including the nanometer range.[73] In view of very low gas solubilities in bulk water, the existence of eventual short-range effects would be indicative of considerable surface adsorption of the gas. Likewise, our estimates of dissolved N_2 effects on the ease of water expulsion from a hydrocarbon-like confinement show[41] that the anticipated[69] reduction in the pertinent activation barrier is insignificant unless the concentration of the gas can exceed the bulk solubility by two orders of magnitude.

Despite its potential influence on the hydrophobic effect, and relevance in several other contexts, as diverse as decompression sickness[82] and particle flotation,[83,84] we are not aware of simulation data for gas adsorption in narrow confinements. We need to establish at what conditions the adsorption layers on adjacent surfaces can feel each other and whether this can enhance adsorption in a cooperative manner. Our studies have also been motivated by a couple of recent experiments studying the effects of deaeration on hydrophobic hydration and interaction. Dynamic surface-force apparatus measurements show a dramatic gas effect at long range (above 5 nm), but the effect is minimal at close range and in determining the adhesion force or interfacial energy.[72] Neutron reflectivity measurements, on the other hand, reveal gas-specific depletion at hydrophobic/water interfaces.[73] Gas-specific effects are also known from measured colloidal stability of hydrophobic particles.[62] However, if such gas-specific effects are present at hydrophobic/water interfaces, interfacial tension would have to vary with deaeration. Dynamic force measurements[72] indicate the opposite. Our calculations are aimed at shedding light on this conundrum.

On the molecular level, adsorption in a narrow confinement can be studied by open ensemble simulations[85] that allow the exchange between the confinement and the bulk phase for both the solvent and gas molecules. In this paper, we describe a semigrand ensemble[85,86] simulation study of adsorption of N_2 and CO_2 in narrow hydrocarbon confinements using a model carefully characterized in previous studies[34,87,88] of solute-free aqueous confinements. We consider nitrogen because it represents the main component in the atmosphere and is not expected to behave very differently from oxygen, and CO_2, which is of interest because of its much greater affinity for water. Following the description of our methods, we present our results for the increase in the overall gas solubility within the confinement. The observed extent of adsorption is compared with expected values for uncoupled surfaces at varied separations. We further examine the dependence of gas adsorption on gas fugacity within a narrow slit of the width $D = 1.4$ nm, which barely exceeds the threshold[34,59] of mechanical instability for expulsion of metastable liquid water from the hydrophobic (hydrocarbon-like) pore. We explore the validity of Henry's law in the range from high dilution up to a few moles of gas per kilogram of water, an empirical threshold concentration at which dissolved gas typically triggers expulsion of simulated liquid water from the specified confinement.

We find a notable increase in gas concentration in the confinement relative to the bulk phase. However, for typical atmospheric conditions, the bulk concentrations are very low, leading to only a small reduction in the interfacial tension estimated from the Gibbs adsorption relation. This implies a very weak dependence of surface force on the presence of the gas in water. Our findings are consistent with the recent dynamic surface-force apparatus measurements[72] but do not reveal any significant gas-specific water depletion at hydrophobic/water interfaces in contrast to recent neutron reflectivity measurements.[73] We show that the influence of gas adsorption becomes more dramatic upon exposure to elevated pressures such as those implicated in decompression sickness,[82] in some industrial processes, and possibly in hydrothermal environments.

II. Model and Method

Water molecules are represented according to the simple-point-charge model[89] (SPC), which describes intermolecular potentials as pairwise sums of Coulombic interactions among atomic charges, q_α, and Lennard-Jones interatom potentials:

$$u_{\alpha\beta}(r) = \frac{q_\alpha q_\beta}{4\pi\epsilon_0 r} + 4\epsilon_{\alpha\beta}\left[\left(\frac{\sigma_{\alpha\beta}}{r}\right)^{12} - \left(\frac{\sigma_{\alpha\beta}}{r}\right)^{6}\right] \qquad (1)$$

Above, the subscripts α and β denote distinct interacting sites in the molecule, and analogous representation is used for dissolved gases (N_2 and CO_2). ϵ_0 is the permittivity of vacuum. Whereas interacting sites in molecular models for H_2O and CO_2 coincide with atom positions, an additional, positively charged site is introduced in the center of the model N_2 molecule to capture the known quadrupolar moment of N_2. Because the solution behavior is dominated by solvent−solute rather than solute−solute interactions,[90−92] in Table 1 we present Lennard-Jones parameters describing pair potentials between a specified atom (α) and the oxygen atom of water (w), $\epsilon_{\alpha w}$, and contact distances, $\sigma_{\alpha w}$, along with atomic charges, q_α, for respective atoms. The remaining interactions follow from usual combining rules $\sigma_{\alpha\beta} = (\sigma_\alpha + \sigma_\beta)/2$ and $\epsilon_{\alpha\beta} = (\epsilon_\alpha\epsilon_\beta)^{1/2}$. Interatomic O−H distances in the SPC model equal 0.1 nm, and the bond angle is $\sim$109.5°. The distance between nitrogen atoms in the N_2 molecule is taken to be 0.11 nm. Distances of C−O in the linear CO_2 molecule equal 0.1162 nm. In analogy with reported studies in bulk CO_2 solutions, the reaction of CO_2 with water is not considered, a simplification that is not believed to have any serious consequences as it affects below 0.5% of CO_2 molecules.[92] In the present work, to focus on the generic confine-

TABLE 1: Lennard-Jones Potential Parameters Describing the Interaction of Different Atomic Species, α (Oxygen, Hydrogen, Carbon, and Nitrogen Atoms in Water (w), Hydrocarbon (h), N_2, and CO_2) with the Oxygen Atom of Water (O_w)[a]

α	$\epsilon_{\alpha w}/J\ mol^{-1}$	q_α/e_o	$\sigma_{\alpha w}/A$	A_α	B_α
O_w	650.2	−0.82	3.1656	0.22	0.965
H_w		0.41			
C_h	649.5	0.0	3.46		
N_{N_2}	505.0	−0.4731	3.282	0.253	0.935
COM_{N_2}		0.9462			
O_{CO_2}	710.6	−0.3086	3.0145	0.143	0.819
C_{CO_2}	513.69	0.6172	3.2618	0.239	0.926

[a] COM denotes the midpoint between nitrogen atoms in the N_2 molecule. q_α is atomic charge. A_α and B_α determine the strengths of the repulsive and attractive atom−wall interactions (eq 3), respectively.

ment effect, we ignore the molecular details of the walls, modeling the hydrophobic confinement by two parallel, perfectly smooth walls with soft weakly attractive wall−water interaction. This interaction follows from integration of the Lennard-Jones (12-6) potential between oxygen atoms of water, O_w, and CH_n groups of the hydrocarbon.[34,87,88] The walls and the confined aqueous film are of infinite lateral size simulated by periodic boundary conditions along directions x and y parallel to the walls. Presuming a uniform number density of hydrocarbon groups, ρ_{C_h}, at all distances $|z| > D_2$, and $\rho_{C_h} = 0$ for $|z| < D_2$, where $D = 2D_2$ is the separation between the two surfaces, the potential energy of a water molecule in the field of the walls is[34]

$$u_w(z) = 4\pi\rho_{C_h}\epsilon_{C_hw}\sigma_{C_hw}^3\left\{\left[\frac{1}{45}\left(\frac{\sigma_{C_hw}}{D_2 - z}\right)^9 - \frac{1}{6}\left(\frac{\sigma_{C_hw}}{D_2 - z}\right)^3\right] + \left[\frac{1}{45}\left(\frac{\sigma_{C_hw}}{D_2 + z}\right)^9 - \frac{1}{6}\left(\frac{\sigma_{C_hw}}{D_2 + z}\right)^3\right]\right\} \quad (2)$$

Analogous relations are used to describe the interaction between the confinement walls and N, C, and O atoms of dissolved N_2 and CO_2. Using respective coupling constants, $\epsilon_{\alpha C_h}$, and contact distances, $\sigma_{\alpha C_h}$, and expressing the distance z relative to the water molecular diameter, σ_w, the reduced atom−wall potentials can be rewritten in a more compact form:

$$\frac{u_\alpha(z)}{k_BT} = A_\alpha\left[\left(\frac{\sigma_w}{D_2 - z}\right)^9 + \left(\frac{\sigma_w}{D_2 + z}\right)^9\right] - B_\alpha\left[\left(\frac{\sigma_w}{D_2 - z}\right)^3 + \left(\frac{\sigma_w}{D_2 + z}\right)^3\right] \quad (3)$$

Room temperature ($T = 298$ K) coupling constants A_α and B_α, describing the repulsive and attractive wall−atom terms, respectively, are collected in Table 1. The resulting water−wall interaction is the same as used in several studies.[34,87,88] Because hydrogen atoms in the SPC model exert no Lennard-Jones interaction, the water−wall potential is effectively a single particle potential that depends only on the position of the water oxygen, regardless of the molecular orientation. The interaction of N_2 and CO_2 molecules with the walls, on the other hand, is orientation dependent. The energy of the system is calculated as a sum of atom−wall interactions and a pairwise sum of interactions between interacting sites on distinct molecules, including interactions among the sites within the simulation box and their images introduced through periodic boundary conditions. In view of prohibitive computational costs of two-dimensional Ewald summations, we follow the procedure of Shelley and Patey[88] with water-water interactions subject to a smooth spherical truncation. Limited comparisons[34] with the results obtained upon inclusion of the two-dimensional Ewald summation[93−95] have revealed no significant differences between the two methods at the conditions of our present study.

To maintain conditions corresponding to the equilibrium between the confined liquid and the adjacent bulk solution, we used open ensemble simulations with fixed temperature, volume, and chemical potentials of water and gas components. The exchange of water molecules between the confinement and the bulk phase was implemented according to the Grand Canonical Monte Carlo (GCMC) algorithm as described previously.[34,41] Using the formalism of Adams,[96,97] the acceptance probabilities for attempted additions and deletions are given by

$$P_{N\to N+1} = \min\left\{1, \frac{\langle N\rangle}{(N+1)} e^{\beta(\mu^{ex} - \Delta U)}\right\} \quad (4)$$

$$P_{N\to N-1} = \min\left\{1, \frac{N}{\langle N\rangle} e^{\beta(-\mu^{ex} - \Delta U)}\right\} \quad (5)$$

where μ^{ex} is the excess chemical potential of water, ΔU is the energy change upon addition or deletion of a molecule, and $\langle N\rangle$ is the average number of molecules occupying the simulation box of given thickness D at bulk phase conditions. To improve exchange acceptances for somewhat bulkier gas molecules, the latter were added or deleted according to the semigrand (SGCMC) or reaction ensemble (REMC)[85,86,98] sampling. This method incorporates changes in the chemical identity of particles. The acceptance probability of an attempted exchange of water and gas molecules is easily determined as the product of acceptance probabilities for the deletion of a randomly chosen water molecule and subsequent addition of a randomly oriented gas molecule at the same position, as given by eqs 4 and 5:

$$P_{w\to g} = \min\left\{1, \frac{N_w}{\langle N_w\rangle}\frac{\langle N_g\rangle}{(N_g+1)} e^{\beta(\mu_g^{ex} - \mu_w^{ex} - \Delta U)}\right\} \quad (6)$$

By analogy, the acceptance probability for the reverse process where a gas molecule is traded for molecule of water is

$$P_{g\to w} = \min\left\{1, \frac{N_g}{\langle N_g\rangle}\frac{\langle N_w\rangle}{(N_w+1)} e^{\beta(\mu_w^{ex} - \mu_g^{ex} - \Delta U)}\right\} \quad (7)$$

It is easy to show the equivalence of eqs 6 and 7 and the relation

$$P_{w\to g;\xi} = \min\left\{1, \frac{N_g!}{(N_g+\xi)!}\frac{N_w!}{(N_w-\xi)!} e^{\beta(\mu_w^0 - \mu_g^0 - \Delta U)}\right\} \quad (8)$$

Equation 8 is equivalent to a more general eq 18 of ref 86, here rewritten to apply to the particular molecular exchange. ξ equals 1 for the forward and −1 for the reverse exchange, $\mu_\alpha^0 - \mu_\beta^0 = \mu_\beta^{ex} - \mu_\alpha^{ex} + k_BT \ln\langle N_\beta\rangle/\langle N_\alpha\rangle$ is the standard free energy of the reaction $\alpha \to \beta$, and $\langle N_\beta\rangle/\langle N_\alpha\rangle$ is the bulk phase concentration ratio of the two species at equilibrium. The excess chemical potential for SPC water at the simulation temperature $T = 298$ K, $\beta\mu_w^{ex} = -10.596$, has been determined in previous work[34] and is in good agreement with the reported result for SPC/E water, $\beta\mu_w^{ex} = -10.7$.[99] The corresponding values for the two gases,[100] $\beta\mu_{N_2}^{ex} = 4.14$ and $\beta\mu_{CO_2}^{ex} = 0.19$, were calculated from the measured Henry constants in water, $K_{N_2} = 8.66 \times 10^4$ bar and $K_{CO_2} = 1.64 \times 10^3$ bar. At gas fugacity $f = 1$ bar, the saturated gas molalities are 6.5×10^{-4} and 0.034 mol kg_w^{-1}, respectively. With given choices of excess chemical potentials,

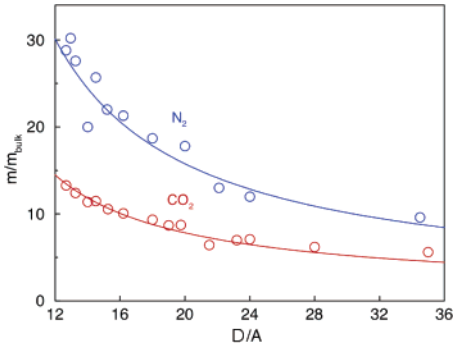

Figure 1. Increase in the average molalities of dissolved gases, N_2 and CO_2, as functions of the width, D, of the hydrocarbon-like confinement. Solid curves describe the predictions of eq 11 based on the surface excess Γ determined at the pore width $D = 1.4$ nm.

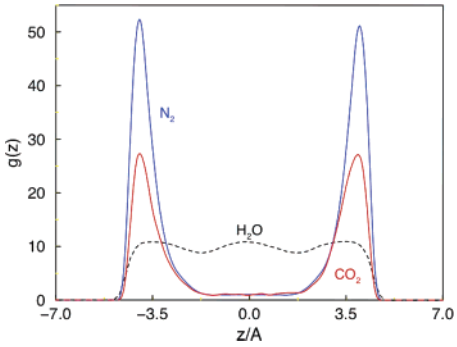

Figure 2. Distribution functions for gas and water molecules in a hydrocarbon-like confinement of width $D = 1.4$ nm, normalized by concentrations in the bulk phase. Data for water (dashed) are multiplied by 10 for easier comparison.

experimental solubilities in the bulk phase were reproduced within 10%, confirming the adequacy of model molecular potentials.

Simulations in the confinement were carried out in a rectangular box with lateral size L_{xy} held fixed at 1.8 nm when the confinement width D did not exceed 1.8 nm. At bigger D, the lateral size was increased to maintain approximately cubic geometry of the box. Trial moves (translations and rotations) of particles were attempted in 20% of the attempted configuration changes, and the remaining attempts were used with equal probabilities for GCMC additions or deletions of water molecules and SGCMC exchanges between molecules of gas and water. To secure an acceptable speed of equilibration of distribution profiles and pressures on the two opposite walls, in addition to molecular moves, it proved to be essential to include simultaneous moves of both confinement walls (in perpendicular direction) at fixed wall−wall separation.[34] Inclusion of a small fraction (below 1%) of wall moves (equivalent to collective moves of all confined molecules relative to the walls) accelerated the equilibration of the water distribution by nearly *2 orders* of magnitude. In view of the quite low gas solubilities, equilibration with respect to the gas content was unavoidably very slow with close to 10^9 attempted moves required in a typical calculation of gas absorption to obtain average statistical accuracy in gas molality (estimated from subaverage statistics) better than ±5%.

III. Results and Discussion

Below, we first present the results for gas accumulation in narrow confinements maintaining equilibrium with the bulk aqueous phase saturated with gas of fugacity $f = 1$ bar. In Figure 1 we show the average confinement molalities of N_2 and CO_2 (relative to the saturated bulk phase) as functions of the interwall separation. Here, molality is preferred over concentration as the measure of gas solubility because of somewhat ambiguous definition of the solvent-accessible volume in a soft confinement. Both the extent of adsorption and the concomitant destabilizing effect on the liquid are expected to increase with increasing proximity of the two walls; hence, narrow confinements are our primary interest. From below, the range of interesting confinement widths is limited by the threshold distance of mechanical instability (spinodal) of liquid water between hydrocarbon-like walls,[34,87] previously determined at $D_c \sim 1.3$ nm.[34,59] This separation is sufficient to accommodate about three molecular layers of water.[34] The somewhat smaller critical distance reported recently for confinements with similar, hydrocarbon-like polarity was due to finite lateral size of apolar solutes considered in that study,[45] as predicted by eq 1 of ref 20. As will be shown shortly, the adsorption layers at the opposite walls are uncoupled at separations much smaller than our upper size limit, $D \sim 3.5$ nm. Results for nanoscale distances D therefore suffice to estimate the amount of dissolved gas at arbitrary separation.

The average molality of the dissolved gas is shown to steadily increase as the width of the confinement decreases, reaching ∼30 and 15 times that of the saturated bulk phase in the cases of N_2 and CO_2, respectively. The stronger relative adsorption of N_2 cannot be explained in terms of direct attraction of gas molecules to the hydrocarbon because this attraction is about 30% weaker than in the case of triatomic CO_2 molecules. Instead, it is attributed to relatively weak attractive forces between water and "hydrophobic" N_2 molecules, as reflected in the poor solubility of N_2 relative to CO_2 in water. In ref 41 we have estimated the effect of an inclusion of a single N_2 molecule on the activation barrier of vapor nucleation preceding capillary evaporation. For modest wall−wall separation of 1.4 nm, the reduction in the barrier height of approximately $2k_BT$ has been determined. The probability of gas inclusion in the vapor nucleus at saturated gas concentration of $\sim 10^{-3}$ mol kg is, however, rather low. A considerable effect of dissolved gas on the kinetics of water expulsion from a hydrophobic confinement[41] is therefore not expected unless the gas concentration in the pore can exceed the bulk value by several orders of magnitude.

As the distribution of the gas inside a pore is strongly nonuniform,[41] it is of interest to present gas density profiles at a small wall−wall separation where maximal local concentrations of gas molecules are expected. In Figure 2, we present density profiles for the two gases in aqueous confinements of width $D = 1.4$ nm at gas fugacities $f = 1$ bar. The density profile for aqueous molecules (dashed curve) is included for comparison. According to our calculation, gas concentrations corresponding to atmospheric conditions result in no visible change in the structure of water film in the confinement. All density profiles in Figure 2 are normalized by the bulk value for each component. Calculations performed at varied f show that gas distribution functions depend very weakly on gas fugacity (and concentration) for all fugacities $f_{CO_2} \leq 2$ bar and $f_{N_2} \leq \sim 40$ bar. At higher fugacities, the saturation with gas triggered expulsion of metastable liquid water from the confinement. The invariance of the $g(z)$ observation, as well as the existence of a relatively broad interval around the pore mid-plane with gas density equal to the bulk value, indicates that the two adsorption layers on opposite confinement walls build up essentially independently of each other and are, within the range of practically relevant fugacities, very similar to the case of

adsorption on isolated walls. Spontaneous evaporation of water[11,20,34,41,48] precludes studies of narrower confinements with overlapping adsorption profiles and concomitant cooperativity effects.

In view of the weak dependence of the adsorption profiles on the slit width, D, it is easy to estimate the overall amount of adsorbed gases as a function of wall−wall separation. For the purpose, we first express the surface excess of the gas, Γ, as

$$\Gamma = m_b \rho_w \int_{-D/2}^{0} [g_g(z) - 1]\, dz \qquad (9)$$

where $g_g(z)$ is the wall/gas distribution function, m_b the bulk molality of the gas, and ρ_w the density of water. The average gas molality in the confinement, $\langle m_g(z)\rangle$, compared to the bulk value m_b is

$$\frac{\langle m_g(z)\rangle}{m_b} = 1 + \frac{2\Gamma S}{m_b m_w} \approx 1 + \frac{2\Gamma S}{m_b \rho_w D S} = 1 + 2\frac{\int_{-D/2}^{0} [g_g(z) - 1]\, dz}{D} \qquad (10)$$

where m_w is the mass of aqueous film confined in a slit of width D and lateral area S. With the numerator in the right-hand side of eq 10 approximately independent of D, the relative increase in gas molality in the confinement varies as

$$\frac{\langle m_g(z)\rangle}{m_b} \approx 1 + \frac{C}{D} \quad \text{where } C = 2\int_{-D/2}^{0} [g_g(z) - 1]\, dz \qquad (11)$$

Equation 11 provides an estimate for the extent of gas adsorption at arbitrary width D. Solid curves in Figure 1 are the predictions from eq 11 with constants C for the two gases calculated using density profiles $g_g(z)$ for N_2 and CO_2 from Figure 2. The excellent agreement with the results of open ensemble simulations for the two gases confirms the absence of any significant coupling between adsorption processes on the opposing confinement walls for all relevant pore widths D exceeding the kinetic threshold distance for evaporation, D_c^k (see Figure 1 of ref 48).

Despite a notable relative increase in the amount of dissolved gas in the confinement compared to the bulk solution, at atmospheric conditions, its concentration does not appear to be sufficient to significantly facilitate capillary evaporation of metastable confined liquid. For this to happen, the confinement has to be brought into equilibrium with the reservoir of water saturated with gas at sufficiently increased fugacity. In Figure 3, we compare simulation time dependencies of the numbers of confined water and CO_2 molecules at fugacities f_{CO_2} of 1 and 3 bar. Time is expressed in terms of the number of attempted molecular moves, including additions, deletions, and exchanges. On the basis of the observed mean squared displacement of water molecules, the total observation interval spanned in Figure 3 may be considered to roughly correspond to a ~80 ps simulation run in a molecular dynamics simulation. At the lower gas fugacity, the average number of CO_2 molecules in the simulation box, $\langle N_{CO_2}\rangle$, was close to 0.8 (compared to $\sim 10^2$ aqueous molecules), but occasional fluctuations to 6 or more gas molecules in the box have been observed. It is during such fluctuations when vapor nucleation events become more likely to take place due to the reduction of the activation barrier to nucleation in the presence of gas molecules.[41] However, at CO_2 fugacity of 1 bar, and slit width $D = 1.4$ nm, the liquid phase persisted during accessible simulation times of $>10^9$ attempted moves.

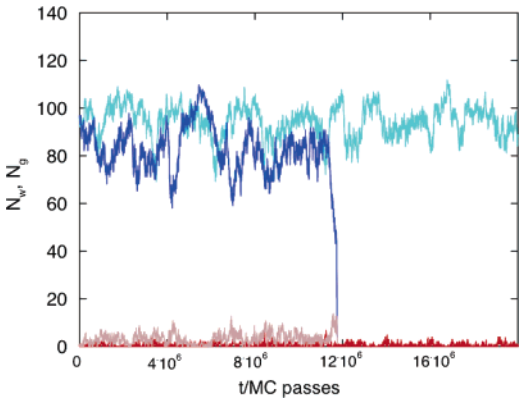

Figure 3. Representative simulation time dependencies of the numbers of water (green, blue) and dissolved CO_2 (brown, red) molecules in a $(1.8\ \text{nm})^2$ section of an oily confinement of width $D = 1.4$ nm at gas fugacities $f = 1$ bar (green, red) or $f = 3$ bar (blue, brown curves). Time variable is the number of attempted simulation moves.

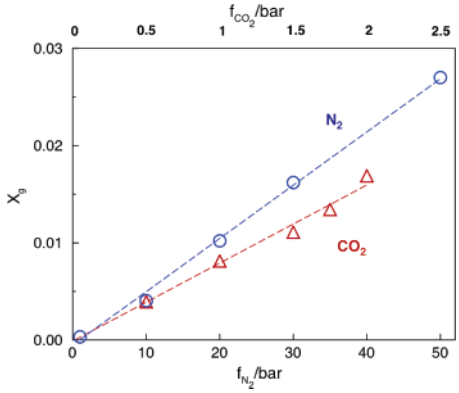

Figure 4. Average mole fractions of N_2 (○) and CO_2 (△) molecules in a hydrophobic confinement of width $D = 1.4$ nm as functions of gas fugacities f.

It is of interest to examine the variation in the gas absorption in the confinement when the gas fugacity is increased in the bulk reservoir. In Figure 4, we present saturated molalities of N_2 and CO_2 in a 1.4 nm slit as functions of gas fugacity. As will be shown shortly, at certain threshold fugacities the amount of adsorbed gas becomes sufficient to lead to capillary evaporation of water in the confinement. In Figure 4, we also include a few data at fugacities exceeding the kinetic threshold for water expulsion. These points correspond to metastable conditions sustained until the evaporation event took place. Interestingly, we find that Henry's law remains approximately valid throughout a wide range of fugacities. The notable increase in gas molality in interfacial systems compared to the bulk phase is of particular relevance at increased pressures such as those involved in diving.[82] Here, adsorption at vessel interfaces and in porous tissues can visibly increase the amount of adsorbed gas to be subsequently released upon decompression. Our equilibrium calculations show that this amount, up to 30 times above the values based on bulk phase solubilities, can be relatively well approximated by the extension of Henry's law to porous material.

In the case of CO_2, fluctuations in the amount of adsorbed gas typically became sufficient to trigger liquid-to-vapor transition when gas fugacity was increased above 2 bar. The two curves corresponding to the numbers of water and CO_2 molecules in a run at $f_{CO_2} = 3$ bar in Figure 3 illustrate an evaporation event that followed a fluctuation in the number of gas molecules in the simulated system, reaching $N_{CO_2} \sim 16$ just

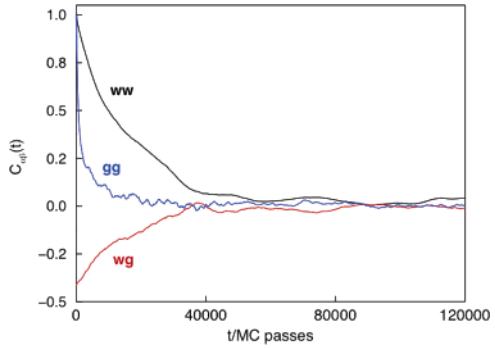

Figure 5. Time correlation functions (eq 12) between the numbers of water (w) and CO_2 (g) molecules in a hydrophobic confinement of width $D = 1.4$ nm in equilibrium with the bulk solution at CO_2 fugacity $f = 1$ bar. Time variable is represented by the number of attempted simulation passes.

before the liquid-to-vapor transition. At given fugacity, the long-time average number $\langle N_{CO_2} \rangle$ in the box prior to evaporation was around 2.4.

With the exception of the states sampled during the evaporation transition, the fluctuations in the numbers of aqueous and gas molecules were found to be strongly correlated. In Figure 5, we compare three correlation functions, $C_{N_wN_w}(t)$, $C_{N_wN_{CO2}}(t)$, and $C_{N_{CO2}N_{CO2}}(t)$, defined as

$$C_{\alpha\beta}(t) = \frac{\langle \delta N_\alpha(t) \delta N_\beta(0) \rangle}{\sigma_{N_\alpha} \sigma_{N_\beta}} \qquad (12)$$

where $\delta N_\alpha(t) = N_\alpha(t) - \langle N_\alpha \rangle$, σ_{N_α} is the variance of N_α, and the variable t denotes the simulation time expressed in the number of attempted simulation passes. Negative values of $C_{N_wN_{CO2}}(t)$ at short times show that fluctuations in the numbers of water and gas molecules, to a large extent, take place at the expense of each other, with average fluctuations in the total number of molecules being smaller than those observed for water alone. Using the connection between the mean square displacement of water molecules and simulation time, the relaxation time of $C_{N_wN_w}(t)$ could be roughly estimated to fall between 2 and 4 ps. Fluctuations in the number of gas molecules appear to take place at a faster time scale, whereas the relaxation of $C_{N_wN_{CO2}}(t)$ occurs within the time scale of $C_{N_wN_w}(t)$. In view of the rapid relaxation of density fluctuations suggesting a quick response in dissolved gas concentration to pressure variation, diffusion and coalescence of interstitial gaseous cavities[101] (initially formed upon decompression) represent the likely rate-limiting processes in the formation of bubbles associated with decompression sickness.[82] Because of ambiguities associated with the correspondence between real and simulation times, including its dependence on the frequency of attempted particle exchanges, it should be noted that the above comparisons serve solely a qualitative purpose; *NPT* Molecular Dynamics simulations of a pore/reservoir system[45,102] could be used to provide more conclusive estimates of concentration fluctuation dynamics in the confinement.

In the case of N_2, because of its low solubility, at ambient pressure the dissolved gas showed no effect on the longevity of the metastable liquid film. At the confinement width $D = 1.4$ nm and typical simulation run lengths of $O(10^9)$ attempted moves, capillary evaporation was typically induced at N_2 fugacities of about 40 bar or higher. This corresponds to the threshold confinement molality ~ 0.8 mol kg_w^{-1}, with the number of N_2 molecules in the simulation cell close to 2, which is similar to the conditions at the gas-induced evaporation threshold in solutions of bulkier but more hydrophilic CO_2 molecules. In either case, the threshold gas concentration is way above typical values for confined solutions saturated at atmospheric conditions. The solubility of the remaining major gas in the atmosphere, oxygen (not considered in this study), is higher than that of N_2; however, this is offset by its lower atmospheric pressure, resulting in comparable concentrations of dissolved O_2 and N_2 upon exposure to air. In addition, O_2 molecules are less hydrophobic (higher solubility compared to N_2) and hence less conducive to water evaporation. A N_2/O_2 mixture mimicking air is therefore not expected to have a significantly different effect from that of N_2 alone.

For the two gases we considered, we find the density profile of the water film in the confinement to be essentially unchanged upon saturation with dissolved gas at atmospheric gas fugacities. Our results therefore indicate that measured effects of atmospheric gases on hydrophobic interaction cannot be attributed to molecular scale events accessible in standard simulation models. This observation, along with SFA and AFM evidence of gas effects on hydrophobic interaction, points to the crucial role of nano- or microbubbles (O(10) nm and higher); such bubbles have indeed been associated[74,75] with situations characterized by long-range and often stepwise interaction profiles,[2,103−105] although alternative explanations have also been proposed.[76] Interestingly, a recent dynamic SFA measurement[72] performed in water confined between hydrophobized mica surfaces, both in the presence of dissolved gases and upon deareation, over a broad range of distances including the nanoscale regime, have indeed demonstrated that the gas effects tend to remain limited to intersurface separations exceeding ~5 nm, consistent with our present findings, but gave no evidence of bubble effects.[72]

In another study of confined aqueous films, neutron reflectivity measurements reveal gas-specific dewetting (water depletion) on hydrophobized quartz/water interfaces.[73] Such surface density depression could be indicative of short-range gas-specific effects on the measured surface force.[22] It is unclear whether the differences in hydrophobic surface coatings, dimethyldioctadecylammonium (DODABr) and octadecyl-trichlorosilane (OTS) used in refs 72 and 73, respectively, can reconcile the apparently different behaviors. Models incorporating full molecular detail of the hydrophobized surfaces would be needed to capture specific interactions of gas molecules with OTS tails, possible swelling of the OTS layer upon gas absorption, or other effects that might contribute to the rather wide surface depletion of interfacial water (about 0.5 nm) suggested by the measurements in ref 73, but not yet seen in any of theoretical calculations that take into account weakly attractive van der Waals water−surface interactions.[30−36] As already suggested in ref 73, the observed density drop may also be interpreted as the averaged effect of occasional bigger density fluctuations[41] next to the surfaces.

On the other hand, because of their mesoscopic size, reported at $\sim 10^2$ nm or bigger, adequate coarse-grained descriptions[30,40] would be required to help unveil the physics of microbubble formation and their role in observed long-ranged surface interactions. Electrostatics has also been suggested as a possible source of measured long-range forces,[4] but this does not explain the strong gas dependence observed in the long-range regime.

Neutron reflectivity measurements of dewetting of OTS-covered quartz[73] in D_2O show an interesting gas-specific behavior. Although Ar is expected to contribute the least among measured gases to interfacial solvent depletion, it is surprising that depletion of Ar-saturated D_2O is 2−3 times smaller than

for degassed D_2O. For this reason, in future studies, we intend to compare Ar[106] with other gases using a full-atom model of the hydrophobized surface. This way, we will be able to distinguish between a genuine gas-specific effect and the possibility that Ar is associated with displacing the air that could remain trapped within the micropockets on the coated surfaces [64,76] despite vacuum degassing.

IV. Concluding Remarks

To shed light on the effects of dissolved gases on measured hydrophobic forces and possible water depletion on hydrophobic surfaces, we used open ensemble simulations to study the adsorption of atmospheric gases, N_2 and CO_2, in hydrophobic confinements. We find considerable accumulation of gas molecules at paraffin-like surfaces, with close to 50- or 25-fold increases in local concentrations next to the surface compared to respective concentrations in bulk phases. Adsorption is, however, restricted to the first monolayer even in very narrow confinements that can accommodate as few as three to four layers of water molecules. Because of low concentrations of atmospheric gases in air-saturated solutions at ambient conditions, the mole fraction of gas molecules at the solid−liquid interface remains below a fraction of a percent, too low to produce noticeable changes on water density structure or to visibly influence the competition between liquid and vapor phases of water in the confinement. Our observations agree with dynamic SFA measurements that find no short-range (below ~5 nm) gas effects on hydrophobic force even when the effect is very strong in the long-range regime.[72] Interestingly, a different picture is suggested by neutron reflectivity measurements at similar conditions showing notable gas-specific effects on surface depletion of water on hydrophobized surfaces.[73] Our model calculations do not reproduce this depletion.

A linear dependence of gas adsorption in the confinement on its fugacity is observed over the whole range of accessible fugacities. On the basis of our simulations, fugacities exceeding 40 bar for N_2 and 2 bar for CO_2 are needed to trigger expulsion of simulated water from a 1.4 nm wide paraffin-like confinement within accessible simulation times, which roughly correspond to the nanosecond regime. In view of the steep increase of activation barriers to evaporation with interplate separation,[48] for only slightly wider gaps, it appears that these requirements can safely be generalized to experimental laboratory times. The phase behavior of confined water is therefore not likely to be affected by equilibrium concentration of dissolved gases from air at ambient conditions. This does not rule out possible effects of air *in excess* of saturation concentration, released from hydrophobic surface coatings where it may have remained trapped since their preparation.[64]

Acknowledgment. We thank Kevin Leung for critical reading of the manuscript and the National Science Foundation for financial support through Awards CHE-0211626 and CHE-0512131 (to A.L.) and BES-0432625 (D.B.).

References and Notes

(1) Israelachvili, J. N. *Intermolecular and Surface Forces*; Academic: London, U.K., 1992.
(2) Christenson, H. K.; Claesson, P. M. *Adv. Colloid Interface Sci.* **2001**, *91*, 391.
(3) Lin, Q.; Meyer, E. E.; Tadmor, M.; Israelachvili, J. N.; Kuhl, T. L. *Langmuir* **2005**, *21*, 251.
(4) Meyer, E. E.; Lin, Q.; Hassenkam, T.; Oroudjev, E.; Israelachvili, J. N. *Proc. Natl. Acad. Sci. U.S.A.* **2005**, *102*, 6839.
(5) Weeks, J. D. *Annu. Rev. Phys. Chem.* **2002**, *53*, 533.
(6) Hummer, G.; Garde, S.; Garcia, A. E.; Pratt, L. R. *Chem. Phys.* **2000**, *258*, 349.
(7) Stillinger, F. H. *J. Solution Chem.* **1973**, *2*, 141.
(8) Berne, B. J. *Proc. Natl. Acad. Sci. U.S.A.* **1996**, *93*, 8800.
(9) Borstnik; Robinson, G. W.; Haymet, A. D. J.; et al. *Faraday Discuss.* **1996**, 203.
(10) Hummer, G.; Garde, S.; Garcia, A. E.; Paulaitis, M. E.; Pratt, L. R. *J. Phys. Chem. B* **1998**, *102*, 10469.
(11) Lum, K.; Chandler, D.; Weeks, J. D. *J. Phys. Chem. B* **1999**, *103*, 4570.
(12) Teixeira, J.; Luzar, A. In *Hydration Processes in Biology*; IOS Press: Washington, DC, 1999; Vol. 103, p 35.
(13) Southall, N. T.; Dill, K. A. *J. Phys. Chem. B* **2000**, *104*, 1326.
(14) Rajamani, S.; Truskett, T. M.; Garde, S. *Proc. Natl. Acad. Sci. U.S.A.* **2005**, *102*, 9475.
(15) Luzar, A.; Svetina, S.; Zeks, B. *Chem. Phys. Lett.* **1983**, *96*, 485.
(16) Lee, C. Y.; McCammon, J. A.; Rossky, P. J. *J. Chem. Phys.* **1984**, *80*, 4448.
(17) Du, Q.; Superfine, R.; Freysz, E.; Shen, Y. R. *Phys. Rev. Lett.* **1993**, *70*, 2313.
(18) Richmond, G. L. *Annu. Rev. Phys. Chem.* **2001**, *52*, 357.
(19) Berard, D. R.; Attard, P.; Patey, G. N. *J. Chem. Phys.* **1993**, *98*, 7236.
(20) Lum, K.; Luzar, A. *Phys. Rev. E* **1997**, *56*, R6283.
(21) Patey, G. N. *Ber. Bunsen-Ges.-Phys. Chem. Chem. Phys.* **1996**, *100*, 885.
(22) Forsman, J.; Jonsson, B.; Woodward, C. E.; Wennerstrom, H. *J. Phys. Chem. B* **1997**, *101*, 4253.
(23) Luzar, A.; Bratko, D.; Blum, L. *J. Chem. Phys.* **1987**, *86*, 2955.
(24) Bratko, D.; Blum, L. A Molecular Model for Aqueous Solutions. In *Hydrogen Bonded Liquids*; NATO ASI Series; Dore, J., Teixeria, J., Eds.; Kluwer: Amsterdam, The Netherlands, 1991; p 6367.
(25) Wallqvist, A.; Berne, B. J. *J. Phys. Chem.* **1995**, *99*, 2893.
(26) Hayashi, T.; Pertsin, A. J.; Grunze, M. *J. Chem. Phys.* **2002**, *117*, 6271.
(27) Ball, P. *Nature* **2003**, *423*, 25.
(28) Weeks, J. D.; Selinger, R. L. B.; Broughton, J. Q. *Phys. Rev. Lett.* **1995**, *75*, 2694.
(29) Katsov, K.; Weeks, J. D. *J. Phys. Chem. B* **2001**, *105*, 6738.
(30) Luzar, A.; Leung, K. *J. Chem. Phys.* **2000**, *113*, 5836.
(31) Rudich, Y.; Benjamin, I.; Naaman, R.; Thomas, E.; Trakhtenberg, S.; Ussyshkin, R. *J. Phys. Chem. A* **2000**, *104*, 5238.
(32) Wallqvist, A.; Gallicchio, E.; Levy, R. M. *J. Phys. Chem. B* **2001**, *105*, 6745.
(33) Ashbaugh, H. S.; Paulaitis, M. E. *J. Am. Chem. Soc.* **2001**, *123*, 10721.
(34) Bratko, D.; Curtis, R. A.; Blanch, H. W.; Prausnitz, J. M. *J. Chem. Phys.* **2001**, *115*, 3873.
(35) Huang, D. M.; Chandler, D. *J. Phys. Chem. B* **2002**, *106*, 2047.
(36) Ashbaugh, H. S.; Pratt, L. R.; Paulaitis, M. E.; Clohecy, J.; Beck, T. L. *J. Am. Chem. Soc.* **2005**, *127*, 2808.
(37) Jensen, T. R.; Jensen, M. O.; Reitzel, N.; Balashev, K.; Peters, G. H.; Kjaer, K.; Bjornholm, T. *Phys. Rev. Lett.* **2003**, 90, 086101.
(38) Mao, M.; Zhang, J. H.; Yoon, R. H.; Ducker, W. A. *Langmuir* **2004**, *20*, 1843.
(39) Yushchenko, V. S.; Yaminsky, V. V.; Shchukin, E. D. *J. Colloid Interface Sci.* **1983**, *96*, 307.
(40) Leung, K.; Luzar, A. *J. Chem. Phys.* **2000**, *113*, 5845.
(41) Leung, K.; Luzar, A.; Bratko, D. *Phys. Rev. Lett.* **2003**, 90, 065502.
(42) Andrienko, D.; Patricio, P.; Vinogradova, O. I. *J. Chem. Phys.* **2004**, *121*, 4414.
(43) Yaminsky, V. V. *Colloids Surf. A−Physicochem. Eng. Aspects* **1997**, *130*, 415.
(44) Yaminsky, V. V. *J. Adhesion Sci. Technol.* **2000**, *14*, 187.
(45) Huang, X. H.; Zhou, R. H.; Berne, B. J. *J. Phys. Chem. B* **2005**, *109*, 3546.
(46) Choudhury, N.; Pettitt, B. M. *J. Am. Chem. Soc.* **2005**, *127*, 3556.
(47) Vaitheeswaran, S.; Yin, H.; Rasaiah, J. C. *J. Phys. Chem. B* **2005**, *109*, 6629.
(48) Luzar, A. *J. Phys. Chem. B* **2004**, *108*, 19859.
(49) Israelachvili, J. *J. Vacuum Sci. Technol. A−Vacuum Surf. Films* **1992**, *10*, 2961.
(50) Israelachvili, J. N. *Surf. Sci. Rep.* **1992**, *14*, 109.
(51) Pratt, L. R. *Annu. Rev. Phys. Chem.* **2002**, *53*, 409.
(52) Pratt, L. R.; Pohorille, A. *Chem. Rev.* **2002**, *102*, 2671.
(53) Spalla, O. *Curr. Opin. Colloid Interface Sci* **2000**, *5*, 5.
(54) Zhang, X. Y.; Zhu, Y. X.; Granick, S. *J. Am. Chem. Soc.* **2001**, *123*, 6736.
(55) Kekicheff, P.; Spalla, O. *Phys. Rev. Lett.* **1995**, *75*, 1851.
(56) Zhang, J. H.; Yoon, R. H.; Mao, M.; Ducker, W. A. *Langmuir* **2005**, *21*, 5831.
(57) Gompper, G.; Hauser, M.; Kornyshev, A. A. *J. Chem. Phys.* **1994**, *101*, 3378.

(58) Yaminsky, V. V.; Ninham, B. W. *Langmuir* **1996**, *12*, 4969.
(59) Truskett, T. M.; Debenedetti, P. G.; Torquato, S. *J. Chem. Phys.* **2001**, *114*, 2401.
(60) Meagher, L.; Craig, V. S. J. *Langmuir* **1994**, *10*, 2736.
(61) Ninham, B. W. *Adv. Colloid Interface Sci.* **1999**, *83*, 1.
(62) Gong, W. Q.; Stearnes, J.; Fornasiero, D.; Hayes, R. A.; Ralston, J. *Phys. Chem. Chem. Phys.* **1999**, *1*, 2799.
(63) Mahnke, J.; Stearnes, J.; Hayes, R. A.; Fornasiero, D.; Ralston, J. *Phys. Chem. Chem. Phys.* **1999**, *1*, 2793.
(64) Ishida, N.; Sakamoto, M.; Miyahara, M.; Higashitani, K. *Langmuir* **2000**, *16*, 5681.
(65) Considine, R. F.; Hayes, R. A.; Horn, R. G. *Langmuir* **1999**, *15*, 1657.
(66) Alfridsson, M.; Ninham, B.; Wall, S. *Langmuir* **2000**, *16*, 10087.
(67) Mishchuk, N.; Ralston, J.; Fornasiero, D. *J. Phys. Chem. A* **2002**, *106*, 689.
(68) Pashley, R. M. *J. Phys. Chem. B* **2003**, *107*, 1714.
(69) Wennerstrom, H. *J. Phys. Chem. B* **2003**, *107*, 13772.
(70) Snoswell, D. R. E.; Duan, J. M.; Fornasiero, D.; Ralston, J. *J. Phys. Chem. B* **2003**, *107*, 2986.
(71) Pashley, R. M.; Rzechowicz, M.; Pashley, L. R.; Francis, M. J. *J. Phys. Chem. B* **2005**, *109*, 1231.
(72) Meyer, E. E.; Lin, Q.; Israelachvili, J. N. *Langmuir* **2005**, *21*, 256.
(73) Doshi, D. A.; Watkins, E. B.; Israelachvili, J. N.; Majewski, J. *Proc. Natl. Acad. Sci. U.S.A.* **2005**, *102*, 9458.
(74) Attard, P.; Moody, M. P.; Tyrrell, J. W. G. *Physica A* **2002**, *314*, 696.
(75) Attard, P. *Adv. Colloid Interface Sci.* **2003**, *104*, 75.
(76) Evans, D. R.; Craig, V. S. J.; Senden, T. J. *Physica A* **2004**, *339*, 101.
(77) Beaglehole, D. *J. Phys. Chem.* **1987**, *91*, 5091.
(78) Lubetkin, S. D.; Akhtar, M. *J. Colloid Interface Sci.* **1996**, *180*, 43.
(79) Lum, K.; Chandler, D. *Int. J. Thermophys.* **1998**, *19*, 845.
(80) Craig, V. S. J.; Ninham, B. W.; Pashley, R. M. *Langmuir* **1999**, *15*, 1562.
(81) Christenson, H. K.; Claesson, P. M. *Science* **1988**, *239*, 390.
(82) Vann, R. D.; Thalmann, E. D. *Decompression Physiology and Practice, in The Physiology and Medicine of Diving*; Saunders: London, U.K., 1993.
(83) Paulson, O.; Pugh, R. J. *Langmuir* **1996**, *12*, 4808.
(84) Pugh, R. J.; Weissenborn, P.; Paulson, O. *Int. J. Mineral Process.* **1997**, *51*, 125.
(85) Frenkel, D.; Smit, B. *Understanding Molecular Simulation*; Academic: San Diego, CA, 1996.
(86) Smith, W. R.; Triska, B. *J. Chem. Phys.* **1994**, *100*, 3019.
(87) Lee, S. H.; Rossky, P. J. *J. Chem. Phys.* **1994**, *100*, 3334.
(88) Shelley, J. C.; Patey, G. N. *Mol. Phys.* **1996**, *88*, 385.
(89) Berendsen, H. J. C.; Postma, J. P. M.; van Gunsteren, W. F.; Hermans, J. In *Intermolecular Forces*; Pullman, B., Ed.; Reidel: Dordrecht, The Netherlands, 1981.
(90) Panhuis, M. I. H.; Patterson, C. H.; Lynden-Bell, R. M. *Mol. Phys.* **1998**, *94*, 963.
(91) Somasundaram, T.; Lynden-Bell, R. M.; Patterson, C. H. *Phys. Chem. Chem. Phys.* **1999**, *1*, 143.
(92) Somasundaram, T.; Panhuis, M. I. H.; Lynden-Bell, R. M.; Patterson, C. H. *J. Chem. Phys.* **1999**, *111*, 2190.
(93) Heyes, D. M.; Berber, M.; Clarke, J. H. R. *J. Chem. Soc., Faraday 2* **1977**, *73*, 1485.
(94) Bratko, D.; Henderson, D. J.; Blum, L. *Phys. Rev. A* **1991**, *44*, 8235.
(95) Bratko, D.; Henderson, D. *Phys. Rev. E* **1994**, *49*, 4140.
(96) Adams, D. J. *Mol. Phys.* **1974**, *28*, 1241.
(97) Adams, D. J. *Mol. Phys.* **1975**, *29*, 307.
(98) Lisal, M.; Nezbeda, I.; Smith, W. R. *J. Chem. Phys.* **1999**, *110*, 8597.
(99) Sanchez, I. C.; Truskett, T. M.; In't Veld, P. J. *J. Phys. Chem. B* **1999**, *103*, 5106.
(100) Stone, M. T.; In't Veld, P. J.; Lu, Y.; Sanchez, I. C. *Mol. Phys.* **2002**, *100*, 2773.
(101) Neimark, A. V.; Vishnyakov, A. *J. Chem. Phys.* **2005**, *122*, 054707.
(102) Spohr, E.; Trokhymchuk, A.; Henderson, D. *J. Electroanal. Chem.* **1998**, *450*, 281.
(103) Ederth, T.; Claesson, P.; Liedberg, B. *Langmuir* **1998**, *14*, 4782.
(104) Ederth, T.; Liedberg, B. *Langmuir* **2000**, *16*, 2177.
(105) Ohnishi, S.; Yaminsky, V. V.; Christenson, H. K. *Langmuir* **2000**, *16*, 8360.
(106) Swope, W. C.; Andersen, H. C. *J. Phys. Chem.* **1984**, *88*, 6548.